Journal of Materiomics xxx (xxxx) xxx

Contents lists available at ScienceDirect

Journal of Materiomics

journal homepage: www.journals.elsevier.com/journal-of-materiomics/

Research paper

Size and crystallinity effect on the ultrafast optical response of chemically synthesized silver nanoparticles

Nadzeya Khinevich [a], Domantas Peckus [a, b, *], Asta Tamulevičienė [a, b], Gerda Klimaitė [b], Joel Henzie [c], Tomas Tamulevičius [a, b], Sigitas Tamulevičius [a, b, **]

[a] Institute of Materials Science of Kaunas University of Technology, K. Baršausko St. 59, LT-51423, Kaunas, Lithuania
[b] Department of Physics, Kaunas University of Technology, Studentų St. 50, LT-51368, Kaunas, Lithuania
[c] International Center for Materials Nanoarchitectonics (WPI-MANA), National Institute for Materials Science (NIMS), Tsukuba, 305-0044, Japan

ARTICLE INFO

Article history:
Received 3 July 2023
Received in revised form
21 August 2023
Accepted 22 August 2023
Available online xxx

Keywords:
Silver nanospheres
Silver nanocubes
Electron-phonon coupling
Transient absorption spectroscopy
Crystallite size
Polycrystalline structure

ABSTRACT

The excited localized surface plasmon (LSP) in metallic nanoparticles is known to relax through several processes such as electron-electron scattering, electron-phonon coupling, and phonon-phonon scattering. In the current research, the ultrafast electron-phonon (e-ph) coupling relaxation processes for different average sizes and crystallinity of chemically synthesized silver nanoparticles were evaluated utilizing transient absorption spectroscopy. The nanoparticle size and crystallinity of similar linear dimension polycrystalline spherical and monocrystalline cubic nanoparticles ranging from *ca.* 30–60 nm was related to their electron relaxation time constants and revealed very different dependencies. For the monocrystalline nanocubes, the electron-phonon coupling was not dependent on the cube edge length, while for the polycrystalline nanospheres, it was linearly decreasing with diameter. We demonstrate that the e-ph coupling time constant could be used to evaluate crystallinity and crystallite size in plasmonic metal nanoparticles when the size (surface area) of the nanoparticle is known.

1. Introduction

Metal nanoparticle synthesis and optical characterization have become an important focus in diverse fields from catalysis to sensing and medicine. Special attention is paid to noble metal (Au, Ag, and Pt) nanostructures because they support plasmon resonance. Due to their unique physicochemical properties, Ag NPs are used as biosensor material, additives to composite fibres, cosmetic products, and electronic and optical components [1]. Ag NPs have been one of the most attractive nanomaterials in biomedicine, where they are used for antimicrobial and anticancer therapy, promote wound repair and bone healing, or as an adjuvant to vaccines as an antidiabetic agent [2]. Ag NPs also find multiple applications ranging from heterogeneous catalysis [3] to gas sensing and nonlinear optics [4,5]. Metallic nanoparticles act as a functional base component of nanoscale devices or sensors with high selectivity and sensitivity in these applications. These nanoparticles can also be applied in spectroscopic systems to enhance Raman scattering spectroscopy signal [6]. Nanoscale metal features support localized surface plasmon resonances (LSPs) associated with strong electromagnetic (EM) hotspots. These EM fields enhance the Raman scattering of adsorbed molecules and can be used for chemical sensing [4].

One of the key issues to consider during a variety of applications of metallic NPs includes developments and novel applications in photovoltaics, photodetection, photocatalysis, *etc.* where the LSP excitation of NPs is employed, is their ultrafast optical user-designed response. Currently, there is knowledge of the temporal evolution of hot electrons excited by light and its dependence on the size, composition, and morphology of metal NPs. The excited LSP in metallic NPs is known to relax through several processes such as electron-electron scattering (e-e, typical time scale *ca.* 100 fs), electron-phonon coupling (e-ph, 1–5 ps), and phonon-phonon scattering (ph-ph, 10–100 ps) [7]. When the excitation source is faster than the expansion/contraction period, the light-heated particles can form coherent vibrations called optomechanical

* Corresponding author. Institute of Materials Science of Kaunas University of Technology, K. Baršausko St. 59, LT-51423, Kaunas, Lithuania.
** Corresponding author. Institute of Materials Science of Kaunas University of Technology, K. Baršausko St. 59, LT-51423, Kaunas, Lithuania.
E-mail addresses: domantas.peckus@ktu.lt (D. Peckus), sigitas.tamulevicius@ktu.lt (S. Tamulevičius).
Peer review under responsibility of The Chinese Ceramic Society.

https://doi.org/10.1016/j.jmat.2023.08.009

oscillations that decay together with ph-ph [7–9]. One of the pump-probe spectroscopy variants, transient absorption spectroscopy (TAS) is a primary choice for studying the kinetics of the LSP effect of different processes taking place in femto – to picosecond time scales. Despite intensive research in this field, the thermalization effect of hot electrons in metal NPs with the lattice via electron-phonon coupling, especially the NPs size and shape dependency of the process, has been controversially discussed in recent literature [8,10]. For example, theoretical studies [11] done on the temporal evolution of optically excited conduction electrons in small plasmon-supporting gold and silver NSs predict that the contribution of surface states (and the effect of the size of the NPs) to hot electron dynamics should be relatively small, as surface electrons only make a small fraction of the total conduction electrons for the particle sizes under consideration. In Refs. [8,12] it was experimentally shown that gold and silver NPs do not demonstrate a dependence of hot electron dynamics on size and shape, while copper NPs have shown some dependence on size [13]. Other studies indicated that the e-ph coupling time constants of Ag and Au NPs stop depending on size and shape if the diameter of the NPs becomes greater than 10 nm [8,14,15]. The importance of bulk phonons dependence on the degree of crystallinity of gold NPs was revealed – it was demonstrated that the e-ph coupling time constant increases when polycrystalline gold nanoprisms are annealed and transformed into nearly single-crystal nanospheres (NSs). On the other hand, a size-dependent e-ph coupling time constant was experimentally demonstrated in gold monocrystalline NSs [10]. The larger monocrystalline gold NPs have demonstrated a lower e-ph coupling time constant, which was explained as a result of the decreasing effect of electron-surface scattering and e-ph coupling constants approaching the values reported for bulk gold. Furthermore, the size dependences were outweighed by the effective scattering at grain boundaries [10]. Similar results were reported for gold NPs in Ref. [16] showing no influence of crystallinity on electron-phonon equilibration dynamics. It was suggested that the crystal twins present in the polycrystalline gold NPs do not significantly enhance the e-ph scattering.

Despite the manifold plasmonics-related applications of Ag NPs, the dependence of the e-ph interaction on crystallinity are almost not considered in the literature for Ag NPs in comparison to Au NPs. Studies of the dependence of e-ph coupling on size have been done for a long time [13,17,18] and in most cases no significant size effect was found [13,17–20]. This indicates that e-ph coupling dependence on size is very unlikely in Ag NPs. Nevertheless, in these articles, the crystalline structure was not examined; therefore, it is hard to discriminate between the size and crystallinity influence, which is being tackled in this work. In our studies, the difference in Ag NPs crystallinity was implied by the use of two different wet chemistry methods (reduction of silver salt and polyol synthesis).

Different preparation methods have been reported for the production of Ag NPs, including physical (laser ablation, sputtering, *etc.*), chemical (chemical reduction, green synthesis), photochemical methods, and microwave processing [1]. One of the popular methods used to produce silver nanospheres (Ag NSs) is the reduction of silver salt. In this method, monodisperse Ag NSs are synthesized via the reduction of silver nitrate using a mixture of two chemical agents: sodium citrate (SC) and tannic acid (TA). Combining SC and TA forms a complex with better reducing and stabilizing properties than SC and TA alone [21–23]. Whereas the polyol synthesis method is frequently utilized when non-spherical geometries are preferred, such as nanocubes (NCs), nanowires [24], *etc*. The method provides better control of the crystallinity and geometry of monocrystalline nanocubes (NC) and various polyhedrons were obtained [25,26].

In the current research, we have performed a systematic analysis of ultrafast processes taking place in highly monodispersed polycrystalline and monocrystalline Ag NPs colloids, investigating their LSP relaxation kinetics empowering TAS as a perspective tool for nanomaterial characterization. We explored the dependence of Ag nanoparticle shape, average size, and crystallinity on e-ph coupling. The e-ph coupling of single-crystal Ag NCs was size-invariant while e-ph coupling in polycrystalline Ag NSs had a linear size dependence.

2. Experimental section

2.1. Materials

Silver salt ($AgNO_3$), tannic acid (TA, $C_{76}H_{52}O_{46}$), and trisodium citrate (TC, $Na_3C_6H_5O_7$), 1,5-pentanediol, copper (II) chloride dihydrate ($CuCl_2{\cdot}2H_2O$), poly (vinylpyrrolidone) (PVP, M_w = 55,000 amu) were purchased from Sigma Aldrich and used without further purification. All solutions were prepared with Milli-Q water.

The synthesis of silver nanospheres (sequence a) was carried out according to the procedure developed by N. Bastus [23], where a complex of TA and TC is used and allows control over the nucleation, growth, and stabilization processes, leading to reproducible monodisperse Ag NSs. The method consists of two preparation steps: synthesis of silver seeds followed by growth of Ag NSs.

Synthesis of silver seeds. An aqueous solution (100 mL) containing 5 mmol/L TC and 0.012,5 mmol/L of TA was heated at 100 °C degrees for about 15 min under vigorous stirring. Subsequently, 1 mL of the silver salt solution (25 mmol/L) was injected. The synthesis lasted for 70 min.

Growth of Ag NSs. 19.5 mL of seeds were mixed with 16.5 mL of water and heated under 90 °C, 250 μL of 2.5 mmol/L TA, 100 μL of 25 mmol/L TC, and 250 μL of 25 mmol/L $AgNO_3$ were sequentially injected. After 30 min of heating, 1 mL of aliquots was extracted for further characterization. The solution produced was used as the seed solution for the subsequent synthesis step. The growth process was repeated four times. Aliquots were centrifuged at 7,000 r/min.

Monodisperse solutions of Ag nanocubes (sequence b) were prepared using a modified procedure based on the polyol synthesis method described in Refs. [26,27]. A copper chloride solution was prepared by dissolving 80 mg of $CuCl_2$ in 10 g of 1,5-pentanediol (PD; Acros). Then the two precursor solutions were prepared by dissolving 0.4 g of polyvinylpyrrolidone (PVP; Sigma-Aldrich) in 20 g of PD, and dissolving 35 μL of the above $CuCl_2$ solution and 0.4 g of $AgNO_3$ into 20 g of PD. Next, a 100 mL round bottom flask (RBF) was filled with 20 g of PD and heated to an internal temperature of 130 °C. Once the PD reached this temperature, 500 μL of the $AgNO_3$ solution was added to the RBF, then 30 s later 500 μL of the PVP solution was added to the RBF. This process was repeated every minute (*i.e*. Add the Ag^+ solution at 0:00, the PVP solution at 0:30, then Ag^+ at 1:00 and so on) until the desired nanocube size was achieved.

2.2. Analysis methods

UV–Vis absorbance spectra of the studied nanoparticles were recorded using a fibre-optic spectrometer AvaSpec-2048 (Avantes, The Netherlands) with a resolution of 1.2 nm in the 400–800 nm spectral range.

Transmission electron microscope (TEM) Tecnai G2 F20 X-TWIN (FEI, The Netherlands) with an FE source operated at 200 kV was used for the visualization of Ag NSs. 20 μL of the precipitates after centrifugation were dropped onto a TEM copper mesh and left to dry at room temperature. While Ag NCs were inspected with 2100F (JEOL) TEM operating at 200 kV.

The images were analyzed with ImageJ software and used for the estimation of the mean diameter/edge length and size distribution. For each sample, at least 50 NPs were measured to evaluate the mean diameter (D_M) and standard deviation (SD) - dispersity of the ensemble.

The X-ray diffraction method was used to study the crystalline structure of synthesized Ag NPs. The D8 Discover (Bruker AXS GmbH) diffractometer with a Cu $K_{\alpha 1}$ (λ = 0.154 nm) radiation source and parallel beam focusing geometry was used. Peak intensities were measured in the 30°−90° $2\theta-\theta$ with 0.012° step size. The DIFFRAC.EVA software was used to process the diffractograms. Considering that in all cases single-phase compounds were obtained, we performed the Rietveld refinement using X'pert HighScore Plus software to calculate crystallite sizes and lattice parameters based on Scherrer formula.

Transient absorption spectroscopy was used to study the ultrafast electron dynamics of Ag NPs. The HARPIA spectrometer (Light Conversion, Lithuania) was used for the TAS measurements. For the sample excitation with an ultrafast 290 fs pulse length and 1,030 nm wavelength Yb:KGW laser Pharos (Light Conversion, LT) with a regenerative amplifier at a 66.7 kHz repetition rate was used. Collinear optical parametric generator Orpheus and harmonic generator Lyra (Light Conversion, LT) were used to tune the pump beam wavelength to 350 nm with an excitation intensity of 0.6−13.6 μJ/cm^2, and a pulse width of about 290 fs. The samples of Ag NPs were probed with a white-light supercontinuum generated using a 2 mm thickness sapphire plate excited with the second harmonic (515 nm) of fundamental laser wavelength. The spectral range of the supercontinuum probe, as well as the detection range of the TAS signal relaxation dynamics, spanned wavelengths from 370 nm to 674 nm. The excitation beam was focused on a *ca.* 700 μm diameter spot, while the diameter of the spatially overlapped supercontinuum probe was *ca.* 500 μm [28].

3. Results and discussion

3.1. Properties of synthesized Ag NPs

The process of seeded growth chemical synthesis was repeated and after each growth cycle, Ag nanospheres of different sizes were obtained. The method based on a seed-growth approach allowed us the production of long-term stable aqueous colloidal Ag NS dispersions with narrow size distribution. The homogeneous growth of Ag seeds was kinetically controlled by adjusting the reaction parameters: concentrations of reducing agents, temperature, a silver precursor-to-seed ratio, and pH value as it was proposed in Ref. [23]. From the TEM analysis (Fig. 1) it was determined that Ag NSs diameters after the 1st growth process were 27.8 nm (noted as sample a1) and ranged to 56.6 nm (a4) after the 4th cycle. TEM microscopy analysis also revealed the polycrystalline structure of the Ag NSs (Fig. 1: a−d), while Ag nanocubes are monocrystalline structures (Fig. 1: e−h).

The increasing linear dimension was accompanied by the expected redshift of the absorbance peak (Fig. 2 a, c) related to the dipolar LSP resonance mode and the emergence of the second peak in the UV region associated with the quadrupole mode in larger Ag NSs (Fig. 2a) and Ag NCs (Fig. 2c). The mean diameter (D_M) and standard deviation (SD) of the synthesized Ag NSs, Ag NCs along with their size distribution are depicted in Fig. 2b and d, respectively.

3.2. Crystallinity analysis of Ag NPs

For each sample, the crystallite size and its standard deviation of the NPs were evaluated from the XRD patterns (Fig. 3) which show the diffraction peaks at $2\theta = 38.2°, 44.5°, 64.6°$, and $77.6°, 81.7°$ that correspond to the planes (111), (200), (220), (311), and (222) respectively of the face-centered cubic (FCC) silver structure, according to the standard powder diffraction card Joint Committee on Powder Diffraction Standards (JCPDS 04−0783).

The crystallite size was calculated using the Scherrer formula [29], and the results are presented in Table 1. The table includes the mean diameter of NSs and mean edge length of NCs with standard deviations defined from TEM analysis. One can see that for Ag NSs, the Ag NSs crystallite size increases together with the diameter (Table 1) and this is in good agreement with the applied synthesis approach where during the seeds-growth process, Ag ions reduce on the surface of Ag NPs avoiding new nucleation or agglomeration [23]. The growth mechanism enabled the formation of NPs with a controlled crystallite size, which is important in the quantitative studies of electron-phonon scattering, elucidating the effects of electron scattering in grain boundaries. The crystallite size of Ag NCs was bigger than their spherical counterparts and much closer to the linear dimension of the nanoparticles, a similar result was obtained for the monocrystalline silver nanocubes in Ref. [30] and gold nanospheres in Ref. [31].

3.3. Nonlinear optical spectroscopy

3.3.1. Excited-state relaxation dynamics

TAS measurements were employed to characterize Ag NPs, including defectiveness and structure. The TAS measurement data for Ag NSs at different probe wavelengths and different pump excitation intensities are shown in Figs. S1−S5. Electron-phonon coupling (e-ph, τ_1) and phonon-phonon (ph-ph, τ_2) scattering time constants were calculated from the TAS signal decay traces (Figs. S2−S5) by fitting traces at the negative and positive peaks of the TAS spectra using the exponential decay function with one or two components (1) [26,32].

$$I(t) = A_1 e^{-\frac{t}{\tau_1}} + A_2 e^{-\frac{t}{\tau_2}} + I_0 \quad (1)$$

where A_1; A_2 and τ_1; τ_2 are the amplitudes and time constants of decay, respectively, while I_0 represents the background of the TAS signal [32]. The fitting results for Ag NSs are summarized in Table S1, while the Ag NCs data analysis depicted in Figs. S7−S10 are compiled in Table S2.

For the investigation of coupling time constants, pump excitation intensity measurements were performed (Fig. S6 and Fig. S11). From these measurements, the e-ph coupling time constant ($\tau_{e\text{-}ph}$) was extrapolated from τ_1 under 0 excitation intensity as [13,33,34]. The extrapolated e-ph coupling time constants are shown in Table 1.

Damping of the excited state depends on e-ph couping. It varied from 0.69 ps to 0.96 ps for Ag NSs and from 0.85 ps to 1.05 ps for Ag NCs (Table S1). A relatively weak TAS signal relaxation component was observed and that can be attributed to ph-ph scattering whose durations ranged from 10 ps to 206 ps for Ag NSs (Table S1) and 22−73 ps for Ag NCs (Table S2).

The two-temperature model was used for the calculation of the electron-phonon coupling constant [8] and the electron-phonon coupling constant G was found based on the equation [13,33,35]:

$$G = \gamma T_0 / \tau_{e\text{-}ph} \quad (2)$$

where γ equals 65 J·m^{-3}·K^{-2} [36]; T_0 is the ambient temperature (293 K); $\tau_{e\text{-}ph}$ is hot-electron lifetimes (provided in Table 1).

The polycrystalline Ag NSs indicated a decrease in the e-ph coupling time constant with increasing mean diameter (Fig. 4a)

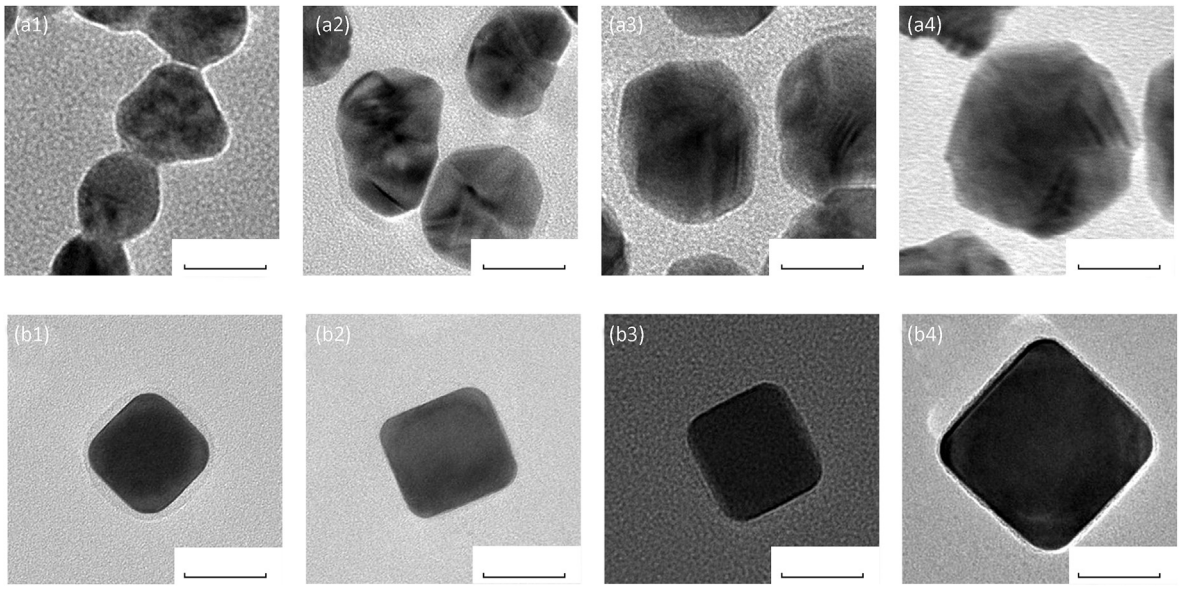

Fig. 1. TEM analysis of the Ag NPs. Top row: Ag nanospheres after 1st process of growth (a1); after 2nd (a2); after 3rd (a3), and after 4th (a4). Bottom row: Ag nanocubes with edge lengths of 32 nm (b1), 35 nm (b2), 37 nm (b3), and 55 nm (b4). The scale bar is 25 nm.

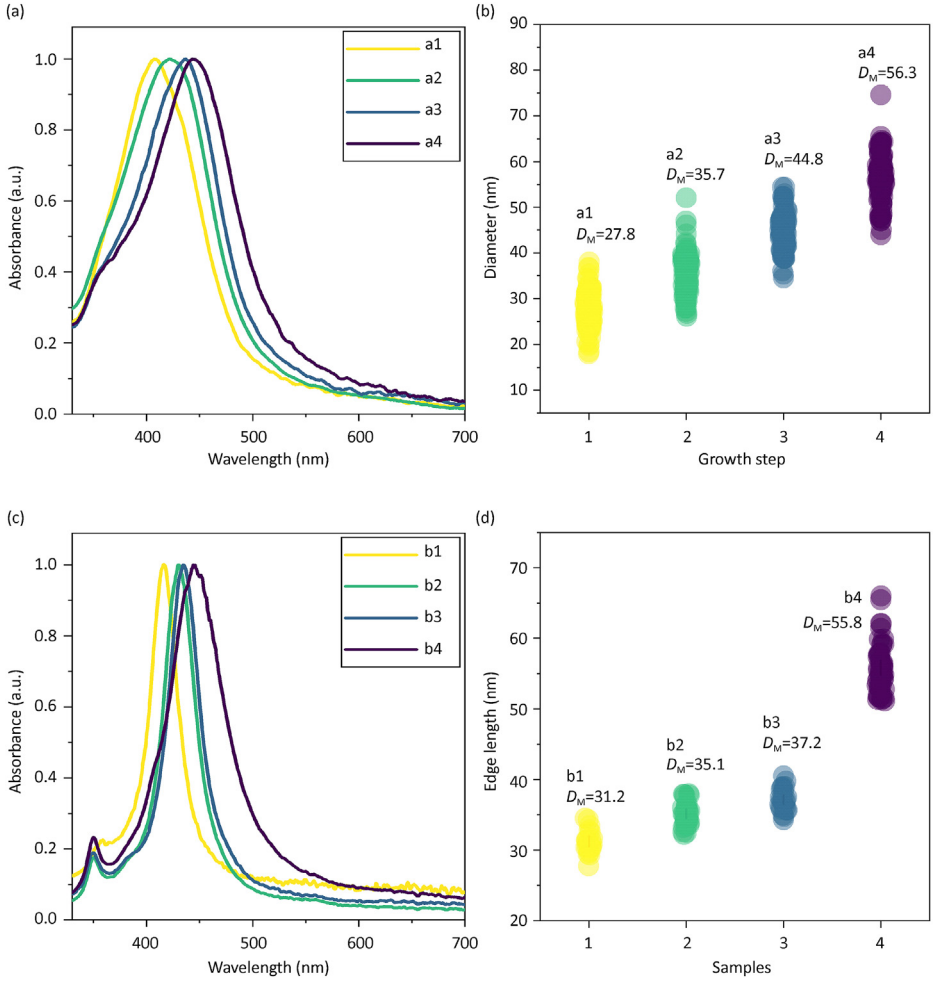

Fig. 2. UV–Vis absorbance spectra (a, c) and size distribution (b, d) of Ag NSs (a, b) and Ag NCs (c, d).

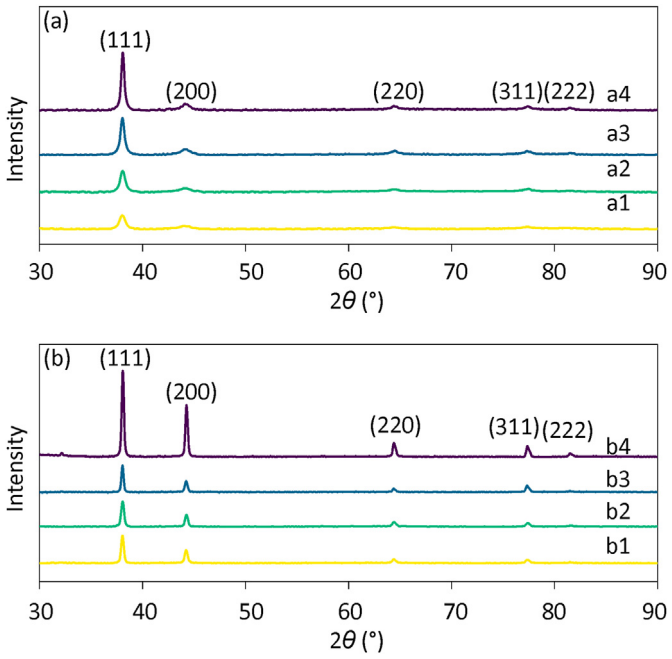

Fig. 3. XRD patterns of Ag NPs: nanospheres (a) and nanocubes (b). The peaks are assigned to diffraction from the planes (100), (200), (220), and (311) of silver (spectra are offset for clarity).

while the monocrystalline Ag NCs seem to be independent of the edge length (Fig. 4a). We also calculated the e-ph coupling time constant dependence on volume of Ag NSs and Ag NCs that corresponds well with data in Fig. 4a (Fig. S12). According to theoretical predictions, the absence of size-dependent e-ph coupling in Au and Ag NPs is due to the relatively small contributions of surface phonon modes to the e-ph coupling process [13] (in case they have a polycrystalline structure [31]). On the other hand, the dependence of the time constant of e-ph coupling on the NPs size has been reported for Cu NPs [13,37] and monocrystalline Au NPs [31]. In these cases, the dependence of the e-ph time constant was attributed to the stronger influence of surface phonon modes on the e-ph coupling process, and the increase in the size of NP has led to longer e-ph coupling time constants. However, this contradicts our obtained dependencies presented in Fig. 4 a. It is also known that the e-ph coupling time depends on the crystallinity of the NPs [33], and the grain boundaries are important to consider in all modes of plasmon damping [31]. To verify this hypothesis, we chose the ratio (Crystallite size/Linear dimension of Ag NPs)^2 (Table 1) for the analysis of the decay time constant of the e-ph coupling, assuming that the higher ratio of crystallite size to the size of NPs corresponds to a more pronounced monocrystalline structure and fewer grain boundaries of the NPs. In this ratio:

$$(\text{Crystallite size/Linear dimension of Ag NPs})^2 \quad (3)$$

Crystallite size – parameter calculated with Scherrer formula from Ag NPs sample XRD data; Linear dimension of Ag NPs – linear dimension is the length picked to evaluate size of Ag NPs. It is diameter for Ag NSs and edge length for Ag NCs. We use Eq. (3) to describe generally both types Ag NPs – for Ag NSs we use eq. (Crystallite size/Diameter of Ag NSs)^2 while for Ag NCs - (Crystallite size/Edge Length of Ag NCs)^2.

The linear dependence of the e-ph coupling decay time constant on (Crystallite size/Diameter of Ag NSs)^2 (Fig. 4b) shows that the e-ph coupling time constant for NSs is size-dependent, and this dependence correlates with the crystallinity of the NP. These findings support the results of other researchers who have shown that the grain boundaries in polycrystalline Au NCs increase the efficiency of coupling of hot electrons with phonons, making the e-ph coupling process faster [12,31]. In this way, the reviled dependence on the time constant e-ph coupling on (Crystallite size/Linear dimension of Ag NP)^2 could in the future be used for control of the crystalline structure of plasmonic metal NPs.

The analysis of e-ph coupling time constants was done for the Ag nanoparticles with sizes that provided us with the most reliable TAS data and therefore the most reliable e-ph coupling time constants. The extension of the range of sizes of samples becomes problematic, because smaller nanoparticles absorb more and scatter less light leading to a strong TAS signal but the smallest samples (below linear size 28 nm) are unstable therefore their time resolved spectroscopy becomes complicated. Investigation of sizes above 60 nm is also challenging because both the absorption and scattering from the nanoparticles prevail and lead to a decrease in TAS signal amplitude and larger noises which makes the calculation of e-ph coupling with huge error margins especially for Ag NSs samples. For comparison we used only Ag NCs that have most similar sizes/volume to Ag NSs. All in all, in our studies we chose to investigate the most reliable results demonstrating Ag nanoparticle sizes for the e-ph coupling time constant analysis. Although we believe that the size range could be extended in the study but some improvements to the synthesis and stability of Ag NSs need to be improved in the future.

4. Conclusion

The chemical synthesis method based on a seed-growth approach applied for the production of long-term stable aqueous colloidal dispersions of spherical silver nanoparticles with narrow, controlled size distribution (mean diameter 28–57 nm), and variable crystallinity proven by TEM, XRD and TAS measurements, allowed systematic studies of the e-ph coupling process in plasmon relaxation dynamics. Comparing similar mean linear dimensions of

Table 1
The mean sizes of Ag NSs (a1–a4) and Ag NCs (b1–b4) based on TEM analysis, crystallite size based on XRD data, electron-phonon coupling time constant $\tau_{e\text{-}ph}$ calculated from TAS data (eq (1)), e-ph coupling constant G based on eq. (2).

Sample	Linear dimension (Diameter/Edge length) (nm)	Crystallite size (nm)	Ratio (Crystallite size/Linear dimension)	Ratio (Crystallite size/Linear dimension)^2	$\tau_{e\text{-}ph}$ (ps)	$G \times 10^{16}$ (W/(m^3·K))
a1	27.8 ± 4.1	9.8 ± 3.1	0.349	0.122	0.96 ± 0.020	1.98
a2	35.7 ± 4.9	10.5 ± 3.8	0.310	0.096	0.90 ± 0.002	2.12
a3	44.7 ± 4.4	13.0 ± 4.8	0.291	0.085	0.77 ± 0.003	2.47
a4	56.6 ± 5.6	15.0 ± 6.6	0.272	0.074	0.69 ± 0.020	2.76
b1	31.3 ± 1.7	27.1 ± 1.4	0.869	0.755	0.86 ± 0.040	2.21
b2	35.1 ± 1.7	27.8 ± 1.9	0.792	0.627	0.94 ± 0.010	2.03
b3	37.2 ± 2.2	30.9 ± 4.5	0.831	0.690	0.85 ± 0.010	2.24
b4	55.8 ± 3.6	32.1 ± 3.8	0.575	0.331	0.85 ± 0.020	2.24

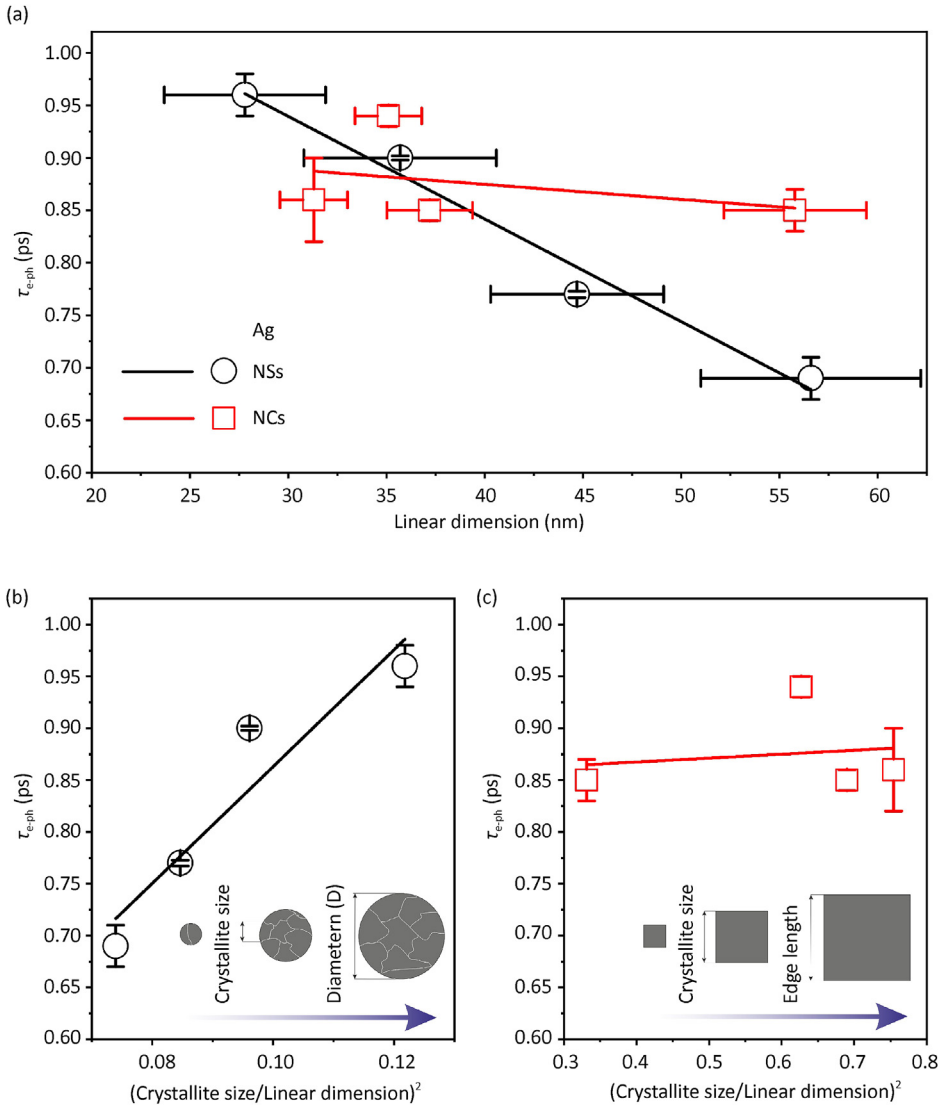

Fig. 4. Dependence of the e-ph coupling time constant ($\tau_{e\text{-}ph}$) on the diameter of Ag NSs and the edge length of the NCs (a). Estimated based on the negative TAS signal, (a), e-ph coupling time constant dependence on (Crystallite size/diameter of Ag NSs)^2 (b); (Crystallite size/edge length of Ag NCs)^2 (c). The black and red lines show the guide for eyes. D – diameter of Ag NSs, EL – edge length of Ag NCs. The insets show schematic image of Ag NSs samples (b) and Ag NCs samples (c).

chemically synthesized polycrystalline and monocrystalline silver particles it was obtained that their electron-phonon relaxation time constants follow different dependencies. The polycrystalline nanoparticles indicated faster relaxation with increasing size, while the decaying of monocrystalline counterparts was indifferent to the size. We have demonstrated that the e-ph coupling decay time constant depends linearly on (Crystallite size/Linear dimension of Ag NPs)^2 for polycrystalline Ag nanospheres, while monocrystalline Ag nanocubes do not show any clear dependence on this ratio. This fact illustrates that e-ph coupling time could be used to evaluate crystallinity and crystallite size in plasmonic metal nanoparticles when the size (surface area) of the nanoparticle is known.

Declaration of competing interest

The authors declare that they have no known competing financial interests or personal relationships that could have appeared to influence the work reported in this paper.

Acknowledgments

The studies were performed within the LaSensA project carried out under the M-ERA.NET 2 scheme (European Union's Horizon 2020 Research and Innovation Program, grant No. 685451) and co-funded by the Research Council of Lithuania (LMTLT), agreement No. S-M-ERA.NET-21-2, the National Science Centre of Poland, project No. 2020/02/Y/ST5/00086, and the Saxon State Ministry for Science, Culture and Tourism (Germany), grant No. 100577922, as well as from the tax funds on the basis of the budget passed by the Saxon state parliament.

Appendix A. Supplementary data

Supplementary data to this article can be found online at https://doi.org/10.1016/j.jmat.2023.08.009.

References

[1] Güzel R, Erdal G. Synthesis of silver nanoparticles. Silver Nanoparticles - Fabr.

Charact. Appl 2018;32:137–44. InTech.
[2] Xu L, Wang Y-Y, Huang J, Chen C-Y, Wang Z-X, Xie H. Silver nanoparticles: synthesis, medical applications and biosafety. Theranostics 2020;10:8996–9031.
[3] Yang Q, Hu M, Guo J, Ge Z, Feng J. Synthesis and enhanced photocatalytic performance of Ag/AgCl/TiO_2 nanocomposites prepared by ion exchange method. J Mater 2018;4:402–11.
[4] Mukherji S, Bharti S, Shukla G, Mukherji S. Synthesis and characterization of size- and shape-controlled silver nanoparticles. Phys. Sci. Rev. 2019;4:20170082.
[5] Zhang J, Zhang B, Yao S, Li H, Chen C, Bala H, et al. Improved triethylamine sensing properties of fish-scale-like porous SnO_2 nanosheets by decorating with Ag nanoparticles. J Mater 2022;8:518–25.
[6] Schlücker S. Surface-Enhanced Raman spectroscopy: concepts and chemical applications. Angew Chem Int Ed 2014;53:4756–95.
[7] Mahmoud MA, O'Neil D, El-Sayed MA. Shape- and symmetry-dependent mechanical properties of metallic gold and silver on the nanoscale. Nano Lett 2015;15. 2764–2764.
[8] Hartland GV. Optical studies of dynamics in noble metal nanostructures. Chem Rev 2011;111:3858–87.
[9] Su M-N, Ostovar B, Gross N, Sader JE, Chang W-S, Link S. Acoustic vibrations and energy dissipation mechanisms for lithographically fabricated plasmonic nanostructures revealed by single-particle transient extinction spectroscopy. J Phys Chem C 2021;125:1621–36.
[10] Staechelin YU, Hoeing D, Schulz F, Lange H. Size-dependent electron–phonon coupling in monocrystalline gold nanoparticles. ACS Photonics 2021;8:752–7.
[11] Saavedra JRM, Asenjo-Garcia A, García De Abajo FJ. Hot-electron dynamics and thermalization in small metallic nanoparticles. ACS Photonics 2016;3:1637–46.
[12] Huang W, Qian W, El-Sayed MA, Ding Y, Wang ZL. Effect of the lattice crystallinity on the Electron–Phonon relaxation rates in gold nanoparticles. J Phys Chem C 2007;111:10751–7.
[13] Darugar Q, Qian W, El-Sayed MA, Pileni MP. Size-dependent ultrafast electronic energy relaxation and enhanced fluorescence of copper nanoparticles. J Phys Chem B 2006;110:143–9.
[14] Arbouet A, Voisin C, Christofilos D, Langot P, Fatti N Del, Vallée F, et al. Electron-phonon scattering in metal clusters. Phys Rev Lett 2003;90:4.
[15] Beane G, Devkota T, Brown BS, Hartland GV. Ultrafast measurements of the dynamics of single nanostructures: a review. Rep Prog Phys 2019;82:016401.
[16] Goubet N, Tempra I, Yang J, Soavi G, Polli D, Cerullo G, et al. Size and nanocrystallinity controlled gold nanocrystals: synthesis, electronic and mechanical properties. Nanoscale 2015;7:3237–46.
[17] Roberti TW, Smith BA, Zhang JZ. Ultrafast electron dynamics at the liquid-metal interface: femtosecond studies using surface plasmons in aqueous silver colloid. J Chem Phys 1995;102:3860–6.
[18] Hodak JH, Martini I, Hartland GV. Spectroscopy and dynamics of nanometer-sized noble metal particles. J Phys Chem B 1998;102:6958–67.
[19] Jiang J, Miao F, Wu W, Kong D, Ridi B, Gao Y. Size effect on nonlinear optical properties and ultrafast dynamics of silver nanoparticles. Opt Express 2022;30:19533.
[20] Maurya SK, Rout A, Ganeev RA, Guo C. Effect of size on the saturable absorption and reverse saturable absorption in silver nanoparticle and ultrafast dynamics at 400 nm. J Nanomater 2019;2019:1–12.
[21] Ranoszek-Soliwoda K, Tomaszewska E, Socha E, Krzyczmonik P, Ignaczak A, Orlowski P, et al. The role of tannic acid and sodium citrate in the synthesis of silver nanoparticles. J Nanoparticle Res 2017;19:273.
[22] Restrepo CV, Villa CC. Synthesis of silver nanoparticles, influence of capping agents, and dependence on size and shape: a review. Environ Nanotechnol Monit Manag 2021;15:100428.
[23] Bastús NG, Merkoçi F, Piella J, Puntes V. Synthesis of highly monodisperse citrate-stabilized silver nanoparticles of up to 200 nm: kinetic control and catalytic properties. Chem Mater 2014;26:2836–46.
[24] Sun Y, Yin Y, Mayers BT, Herricks T, Xia Y. Uniform silver nanowires synthesis by reducing $AgNO_3$ with ethylene glycol in the presence of seeds and poly(-Vinyl pyrrolidone). Chem Mater 2002;14:4736–45.
[25] Henzie J, Grünwald M, Widmer-Cooper A, Geissler PL, Yang P. Self-assembly of uniform polyhedral silver nanocrystals into densest packings and exotic superlattices. Nat Mater 2012;11:131–7.
[26] Peckus D, Rong H, Stankevičius L, Juodenas M, Tamulevičius S, Tamulevičius T, et al. Hot electron emission can lead to damping of optomechanical modes in core-shell Ag@TiO_2 nanocubes. J Phys Chem C 2017;121:24159–67.
[27] Tao A, Sinsermsuksakul P, Yang P. Polyhedral silver nanocrystals with distinct scattering signatures. Angew Chem Int Ed 2006;45:4597–601.
[28] Peckus D, Tamuleviciene A, Mougin K, Spangenberg A, Vidal L, Bauerlin Q, et al. Shape influence on the ultrafast plasmonic properties of gold nanoparticles. Opt Express 2022;30:27730–45.
[29] Patterson AL. The scherrer formula for X-ray particle size determination. Phys Rev 1939;56:978–82.
[30] Helmlinger J, Prymak O, Loza K, Gocyla M, Heggen M, Epple M. On the crystallography of silver nanoparticles with different shapes. Cryst Growth Des 2016;16:3677–87.
[31] Staechelin YU, Hoeing D, Schulz F, Lange H. Size-dependent electron-phonon coupling in monocrystalline gold nanoparticles. ACS Photonics 2021;8:752–7.
[32] Peckus D, Meškinis Š, Vasiliauskas A, Rajackaitė E, Andrulevičius M, Kopustinskas V, et al. Structure and optical properties of diamond like carbon films containing aluminium and alumina. Appl Surf Sci 2020;529:147040.
[33] Huang W, Qian W, El-Sayed MA, Ding Y, Wang ZL. Effect of the lattice crystallinity on the electron-phonon relaxation rates in gold nanoparticles. J Phys Chem C 2007;111:10751–7.
[34] Jain PK, Qian W, El-Sayed MA. Ultrafast electron relaxation dynamics in coupled metal nanoparticles in aggregates. J Phys Chem B 2006;110:136–42.
[35] Lysenko S, Jimenez J, Zhang G, Liu H. Nonlinear optical dynamics of glass-embedded silver nanoparticles. J Electron Mater 2006;35:1715–21.
[36] Bigot J-Y, Halté V, Merle J-C, Daunois A. Electron dynamics in metallic nanoparticles. Chem Phys 2000;251:181–203.
[37] Peckus D, Tamulevičius T, Meškinis Š, Tamulevičienė A, Vasiliauskas A, Ulčinas O, et al. Linear and nonlinear absorption properties of diamond-like carbon doped with Cu nanoparticles. Plasmonics 2016;12:47–58.

Dr. Domantas Peckus, senior researcher at the Institute of Materials Science of Kaunas University of Technology. He has been working with ultrafast transient differential absorption spectroscopy of organic semiconductors, diamond-like carbon, graphene, and plasmonic materials for more than ten years. His research field covers ultrafast excited state relaxation dynamics in organic semiconductors, plasmonic metal nanoparticles, diamond-like carbon and graphene.

Prof. Dr. Habil. Sigitas Tamulevičius, an academician of the Academy of Sciences of Lithuania, a full professor at the Physics Department and Research Director of the Institute of Materials Science of Kaunas University of Technology, obtained the Physics Engineer degree from the Moscow Engineering Institute of Physics (former USSR) in 1979 and a Ph.D. degree from the University of Vilnius in 1984. From 1990 to 1991, he was a postdoctoral researcher at the Royal Institute of Technology (Stockholm, Sweden). In 1994 he was Research Scholar at the Massachusetts Institute of Technology (USA). He has cofounded a spin-off company and co-authored approximately 250 peer-reviewed publications in the field of vacuum and plasma technologies and optical technologies and spectroscopy with more than 2500 citations (h-index: 26 (WoS)). He has received series of awards including the Soros Foundation Research Grant, (1993), Fulbright certificate (1997), National Award for Science (2000 and 2019), Honorary Professor of Southern Denmark University (2020), Laureate of Kaunas City Scientist Award (2017). During 2010–2012, he was a representative member of Lithuania in the EU FP7 committee "Nanoscience, nanotechnologies, materials and novel production technologies".